Biomedical Optics EXPRESS

Handheld Diffuse Reflectance Spectral Imaging (DRSi) for in-vivo characterization of skin

Sheldon F. Bish,[1] Manu Sharma,[1] Youmin Wang,[1] Nicholas J. Triesault,[1] Jason S. Reichenberg,[2] John X.J. Zhang,[1] and James W. Tunnell[1,*]

[1]*Department of Biomedical Engineering, The University of Texas at Austin, 107. W. Dean Keeton St. Austin TX 78712, USA*

[2]*Department of Dermatology, University of Texas Medical Branch, 313 E.12th Street, Austin, Texas 78701, USA*

[*]*jtunnell@austin.utexas.edu*

Abstract: Diffuse reflectance spectroscopy provides a noninvasive means to measure optical and physiological properties of tissues. To expand on these measurements, we have developed a handheld diffuse reflectance spectral imaging (DRSi) system capable of acquiring wide field hyperspectral images of tissue. The image acquisition time was approximately 50 seconds for a 50x50 pixel image. A transport model was used to fit each spectra for reduced scattering coefficient, hemoglobin concentration and melanin concentration resulting in optical property maps. The system was validated across biologically relevant levels of reduced scattering (5.14% error) and absorption (8.34% error) using tissue simulating phantoms. DRSi optical property maps of a pigmented skin lesion were acquired *in vivo*. These trends in optical properties were consistent with previous observations using point probe devices.

OCIS codes: (110.0110) Imaging systems; (110.0113) Imaging through turbid media; (170.6510) Spectroscopy, tissue diagnostics

References and links

1. R. S. Stern, "Prevalence of a History of Skin Cancer in 2007: Results of an Incidence-Based Model," Arch. Dermatol. **146**(3), 279–282 (2010).
2. H. Kittler, H. Pehamberger, K. Wolff, and M. Binder, "Diagnostic accuracy of dermoscopy," Lancet Oncol. **3**(3), 159–165 (2002).
3. J. K. Robinson, "Sun exposure, sun protection, and vitamin D," JAMA **294**(12), 1541–1543 (2005).
4. M. E. Martin, M. B. Wabuyele, K. Chen, P. Kasili, M. Panjehpour, M. Phan, B. Overholt, G. Cunningham, D. Wilson, R. C. Denovo, and T. Vo-Dinh, "Development of an advanced hyperspectral imaging (HSI) system with applications for cancer detection," Ann. Biomed. Eng. **34**(6), 1061–1068 (2006).
5. D. Roblyer, C. Kurachi, A. M. Gillenwater, and R. Richards-Kortum, "In Vivo Fluorescence Hyperspectral Imaging of Oral Neoplasia," in *Advanced Biomedical and Clinical Diagnostic Systems Vii*, A. MahadevanJansen, T. VoDinh, and W. S. Grundfest, eds. (2009).
6. M. G. Müller, I. Georgakoudi, Q. G. Zhang, J. Wu, and M. S. Feld, "Intrinsic fluorescence spectroscopy in turbid media: disentangling effects of scattering and absorption," Appl. Opt. **40**(25), 4633–4646 (2001).
7. T. A. Erickson, A. Mazhar, D. Cuccia, A. J. Durkin, and J. W. Tunnell, "Lookup-table method for imaging optical properties with structured illumination beyond the diffusion theory regime," J. Biomed. Opt. **15**(3), 036013 (2010).
8. B. Yang, M. Sharma, Y. Wang, and J. W. Tunnell, "Attenuation corrected fluorescence extraction using spatial frequency domain imaging system," Proc. SPIE 861809–861809 (2013).
9. C. C. Yu, C. Lau, G. O'Donoghue, J. Mirkovic, S. McGee, L. Galindo, A. Elackattu, E. Stier, G. Grillone, K. Badizadegan, R. R. Dasari, and M. S. Feld, "Quantitative spectroscopic imaging for non-invasive early cancer detection," Opt. Express **16**(20), 16227–16239 (2008).
10. S. A. Burgess, M. B. Bouchard, B. H. Yuan, and E. M. C. Hillman, "Simultaneous multiwavelength laminar optical tomography," Opt. Lett. **33**(22), 2710–2712 (2008).
11. G. Zonios and A. Dimou, "Modeling diffuse reflectance from semi-infinite turbid media: application to the study of skin optical properties," Opt. Express **14**(19), 8661–8674 (2006).
12. M. G. Müller, T. A. Valdez, I. Georgakoudi, V. Backman, C. Fuentes, S. Kabani, N. Laver, Z. M. Wang, C. W. Boone, R. R. Dasari, S. M. Shapshay, and M. S. Feld, "Spectroscopic detection and evaluation of morphologic and biochemical changes in early human oral carcinoma," Cancer **97**(7), 1681–1692 (2003).

#199437 - $15.00 USD Received 14 Oct 2013; revised 6 Dec 2013; accepted 9 Jan 2014; published 24 Jan 2014

13. D. C. G. de Veld, M. Skurichina, M. J. Witjes, R. P. W. Duin, H. J. Sterenborg, and J. L. N. Roodenburg, "Autofluorescence and diffuse reflectance spectroscopy for oral oncology," Lasers Surg. Med. **36**(5), 356–364 (2005).
14. Z. Volynskaya, A. S. Haka, K. L. Bechtel, M. Fitzmaurice, R. Shenk, N. Wang, J. Nazemi, R. R. Dasari, and M. S. Feld, "Diagnosing breast cancer using diffuse reflectance spectroscopy and intrinsic fluorescence spectroscopy," J. Biomed. Opt. **13**(2), 024012 (2008).
15. G. Zonios, L. T. Perelman, V. M. Backman, R. Manoharan, M. Fitzmaurice, J. Van Dam, and M. S. Feld, "Diffuse reflectance spectroscopy of human adenomatous colon polyps in vivo," Appl. Opt. **38**(31), 6628–6637 (1999).
16. J. A. Freeberg, D. M. Serachitopol, N. McKinnon, R. Price, E. N. Atkinson, D. D. Cox, C. MacAulay, R. Richards-Kortum, M. Follen, and B. Pikkula, "Fluorescence and reflectance device variability throughout the progression of a phase II clinical trial to detect and screen for cervical neoplasia using a fiber optic probe," J. Biomed. Opt. **12**(3), 034015 (2007).
17. S. K. Chang, Y. N. Mirabal, E. N. Atkinson, D. Cox, A. Malpica, M. Follen, and R. Richards-Kortum, "Combined reflectance and fluorescence spectroscopy for in vivo detection of cervical pre-cancer," J. Biomed. Opt. **10**(2), 024031 (2005).
18. N. Rajaram, J. S. Reichenberg, M. R. Migden, T. H. Nguyen, and J. W. Tunnell, "Pilot Clinical Study for Quantitative Spectral Diagnosis of Non-Melanoma Skin Cancer," Lasers Surg. Med. **42**(10), 876–887 (2010).
19. N. Rajaram, T. H. Nguyen, and J. W. Tunnell, "Lookup table-based inverse model for determining optical properties of turbid media," J. Biomed. Opt. **13**(5), 050501 (2008).
20. R. Hennessy, S. Bish, J. W. Tunnell, and M. K. Markey, "Segmentation of diffuse reflectance hyperspectral datasets with noise for detection of Melanoma," Conference proceedings: Annual International Conference of the IEEE Engineering in Medicine and Biology Society. IEEE Engineering in Medicine and Biology Society. Conference. **2012**, 1482-1485 (2012).
21. N. Rajaram, D. Kovacic, M. F. Migden, J. S. Reichenberg, T. H. Nguyen, and J. W. Tunnell, "In vivo determination of optical properties and fluorophore characteristics of non-melnoma skin cancer," in *Photonic Therapeutics and Diagnostics V*, N. Kollias, B. Choi, H. Zeng, R. S. Malek, B. J. F. Wong, J. F. R. Ilgner, K. W. Gregory, G. J. Tearney, L. Marcu, H. Hirschberg, and S. J. Madsen, eds. (Spie-Int Soc Optical Engineering, Bellingham, 2009).
22. B. H. Yuan, S. A. Burgess, A. Iranmahboob, M. B. Bouchard, N. Lehrer, C. Bordier, and E. M. C. Hillman, "A system for high-resolution depth-resolved optical imaging of fluorescence and absorption contrast," Rev. Sci. Instrum. **80**(4), 043706 (2009).
23. B. M. Huang, J. Mielikainen, H. Oh, and H. L. A. Huang, "Development of a GPU-based high-performance radiative transfer model for the Infrared Atmospheric Sounding Interferometer (IASI)," J. Comput. Phys. **230**(6), 2207–2221 (2011).

1. Introduction

Over the past 30 years, there has been a higher prevalence of skin cancer than all other cancers combined [1]. Skin cancer screenings, although important, are a highly qualitative and subjective process, suffering from false positives that result in unnecessary invasive biopsies and doctor visits. In fiscal terms, these false positive readings result in an estimated $2B cost to the US health care system and undue stress, pain and disfiguration for the patient. The major factor behind diagnostic accuracy of skin cancer screenings is the clinician's level of experience. Studies have shown that diagnostic accuracy is better for experienced dermatologists than general practitioners [2]. With one in five Americans developing skin cancer in their lifetime [3], there is a growing need to equip healthcare professionals with a tool that will provide *quantitative* as well as qualitative images that can improve on the subjectivity of skin cancer screenings.

For over ten years, optical imaging modalities have been developed that have sought to combine the diagnostic accuracy of spectroscopy with the spatial detail of imaging. Hyperspectral imaging, which involves capturing images of a field under multiple wavelengths, can provide the extraction of biochemical information from tissues, particularly in the presence of multiple absorbers and fluorophores, as is the case in skin. Charge coupled device (CCD) array, or camera based systems acquire snapshots of the skin under different wavelengths of visible illumination in order to build a spectral data cube image where each voxel accounts for a reflectance or fluorescence spectrum. The system developed by Martin *et al*. captured hyperspectral autofluorescence images of a xenograft tumor model *in vivo* [4]. Their system used a liquid crystal tunable filter (LCTF) in concert with an intensified CCD to collect up to 22 wavelength images in a total of 23 seconds. Richards-Kortum *et al*. imaged

#199437 - $15.00 USD Received 14 Oct 2013; revised 6 Dec 2013; accepted 9 Jan 2014; published 24 Jan 2014

oral dysplasia with an LCTF-CCD combination to collect wavelength bands from 400 to 720nm in 5nm increments spanning a duration of 30s-120s [5]. These methods benefit from high spatial resolution offered by CCD arrays, but suffer great losses in optical efficiency primarily due to the polarization of the LCTF. In addition, these studies limit their results to spectral intensity ratios and do not correct for distortions in their fluorescence spectra due to absorption [6]. Without this correction, tumor margin delineated through fluorescence can be obscured by chromophores such as blood, preventing adequate tumor removal.

In another approach to CCD skin imaging, a modality called spatial frequency domain imaging (SFDI) uses structured rather than spectral illumination techniques to derive quantitative maps of optical and physiological properties of turbid media [7, 8]. SFDI uses periodic illumination patterns at different excitation wavelengths on turbid materials and calculates optical properties via evaluation of the modulation transfer function. The advantages of this system are numerous: high spatial resolution; the ability to control optical sampling depth; and structured illumination is used to decouple scattering from absorption.

Recently, point scanning hyperspectral imaging has been extended to relatively large fields of view where reflectance hyperspectral images were obtained by scanning a focused beam of white light across a field and spectrally dispersing the returning diffusely reflected signal. Yu *et al*. was among the first to demonstrate this technique by using scan mirrors to raster scan a white light beam across tissue and de-scan diffusely reflected light that traversed the sampling volume [9]. In their study, the collected spectra of each pixel was fit for reduced scattering and absorption using an analytical model based on the modified diffusion approximation to the radiative transport equation. The merits of this system include high signal to noise (SNR) and spectral resolution; however, the acquisition time was relatively long (90s) and the spatial resolution too low (1mm) for imaging sub-features of skin cancer lesions which are typically 5-10mm in diameter. A design by Burgess *et al*. had a point scanning absorption contrast imaging system with acquisition rates of up to 100 frames per second and was capable of relatively high resolution imaging [10]. However this system only imaged three wavelength bands – red (638nm), green (532nm) and blue (488nm) - rendering it limited for its ability to accurately estimate concentrations of multiple absorbers in biological tissue. Using a hyperspectral imaging approach would reduce the amount of noise and cross talk between absorbtion and scattering cross sections.

Here, we present an handheld raster scanning diffuse reflectance spectroscopic imaging (DRSi) system that uses a well-developed single point optical sampling technique and adapts it to widefield (>10cm^2) imaging. DRSi scans a confined sampling volume defined by the size and center-to-center distance of the source-detector (SD) apertures (Fig. 1).

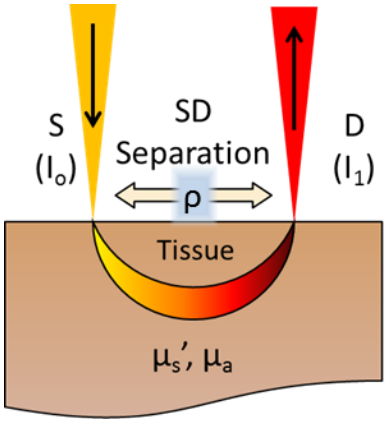

Fig. 1. Sampling geometry of DRSi.

#199437 - $15.00 USD Received 14 Oct 2013; revised 6 Dec 2013; accepted 9 Jan 2014; published 24 Jan 2014

This sampling geometry makes the signal explicitly dependent on reduced scattering and absorption coefficients [11], unlike camera images where the captured signal is a function of albedo ($\mu_s'/(\mu_s' + \mu_a)$). For hyperspectral camera images of turbid media, the lack of spatial confinement makes the separation of μ_s' and μ_a untenable. With DRSi's confined SD apertures, photon path length becomes known, and μ_s' and μ_a can be quantified individually. Single point spectroscopic sampling techniques using optical fibers in contact with the skin (source and collection apertures (SD)) have been used to quantify the reduced scattering and absorption of oral [12, 13], breast [14], colon [15], cervical [16, 17] and skin cancers [18]. This method has been used to classify normal from dysplastic tissues with good sensitivity and specificity when combined with intrinsic fluorescence. By scanning the SD apertures across a wide field, a map of optical and physiological properties can be achieved, which provide meaningful quantitative biological information in a spatially resolved format. DRSi requires that the spectral resolution be adequate to resolve the narrowest spectral features, which are primarily the q-bands of hemoglobin. Spatial resolution in DRSi is limited by the mean free optical scattering path length ($1/\mu_s'$) and the optical sampling geometry. As with single point optical sampling, DRSi uses visible wavelengths where intrinsic chromophores (blood, melanin) absorb with spectrally distinct characteristics.

In this paper, we describe the DRSi system that provides maps of intrinsic biological scattering and absorption properties *in-vivo* without any extrinsic contrast agents. We validate this system for biologically relevant combinations of reduced scattering and absorber concentrations. We characterize the spatial/spectral resolution and signal-to-noise ratio (SNR). We conclude with a clinical demonstration of the system towards the spatio-chemical characterization of skin cancers.

2. Instrumentation and methods

DRSi is a widefield imaging technique with image sizes of over one square centimeter and sampling penetration depths of beyond 1mm, which allows for fast and noninvasive *in vivo* imaging of skin lesions. The diagram shown in Fig. 2 illustrates the basic layout of the DRSi system with the region in pink highlighting the components of the handheld device. This system uses a 75W Xenon arc lamp (Newport, Irvine CA) coupled to a 100μm optical fiber for source power. At the handheld end, light was collimated with a ½" diameter 19mm focal length lens (Thorlabs, Newton NJ) and polarized with a polarizing beamsplitter (Thorlabs, NJ USA.) in order to reject specular reflections. The collimated and polarized source beam was tilted and steered with a pair of galvanometer scanning mirrors (Cambridge Tech., Bedford MA) across a 1" diameter 30mm focal length achromatic for focusing onto the sample. Diffusely reflected light emerging from the tissue surface reverses the optical path through the system. After emerging from the tissue, diffuse reflectance was de-scanned by the galvanometers, and redirected by the beamsplitter down a collection arm where a ½" diameter 19mm focal length lens focuses this light into a 200μm optical fiber for detection. It was important to note that the tip of the source and collection fibers are imaged onto the tissue, forming virtual SD apertures located at ρ microns away from each other. After the diffuse reflectance signal traverses the collection fiber, it reaches the spectrometer (Ocean Optics, Dunedin FL) which was portable and customized for sensitivity in the UV-VIS region of interest. Also to facilitate visualization of skin lesions and co-registration to optical/physiological property maps, the DRSi imager contains a camera, focus-adjusted to snap an image of the sample immediately prior to imaging. For the camera image collection, the field of view was illuminated by an LED ring while a shutter between the beamsplitter and the galvo scanner block the xenon light source from interfering with the image.

#199437 - $15.00 USD Received 14 Oct 2013; revised 6 Dec 2013; accepted 9 Jan 2014; published 24 Jan 2014

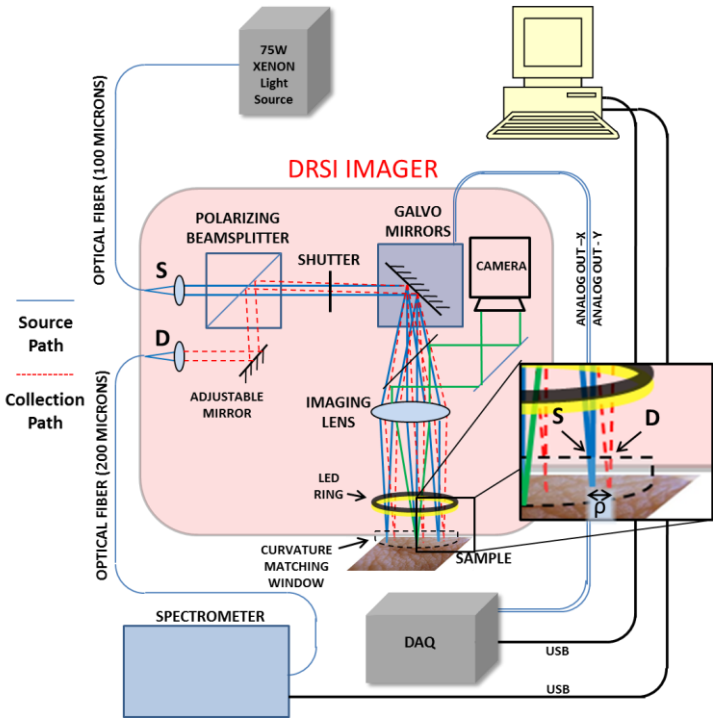

Fig. 2. DRSi System Diagram.

Data acquisition and system automation was performed with LabVIEW (National Instruments, Austin TX) graphical programing software. The system tasks of camera snapshot, shutter and LED control, galvo scanning, hyperspectral image processing and visualization was fully automated to and prevent opportunities for measurement error.

As a result of the scaled-down approach to building a beam-scanning based imaging system, the imaging lens focal length was limited. As a result, this introduces the problem of field curvature and limited depth of field. To address both of these issues, a plano-convex lens was fixed at the focal plane such that the convex surface closely matches the focal plane curvature to ensure that the tissue surface was always in focus. Since this lens functions more as a window, we will call this lens, the 'curvature matching window'. In order to select a plano-convex lens of proper curvature, TracePro imaging simulation software (Lambda Research, MA) was used to optimize the curvature for even distribution of focal spot sizes at all points of scan.

Pre-cancerous and cancerous lesions are commonly found on areas of skin that are contoured and difficult to scan with a large, bulky imaging system. Earlier prototypes of our design were box-like and bulky with the image plane co-incident with the face of the imager body. As a result, lesion images in areas such as the ventral neck, face and lower back were difficult to image and were commonly out of focus. To solve this problem, a customized imager (Fig. 3) was designed from scratch using Solidworks drafting software and constructed using a 3-D printer (EnVisionTec Ultra, Gladbeck Germany). Features of this customized imager are: a tapered neck, facilitating access to more contoured areas of skin; easier access to fiber and electrical connections as well as the collection aperture adjustment knobs; and space efficient housing of optical elements.

#199437 - $15.00 USD Received 14 Oct 2013; revised 6 Dec 2013; accepted 9 Jan 2014; published 24 Jan 2014

Fig. 3. Compact Clinically-Adaptable DRSi Imager and Mobile Cart Setup

The overall clinical presentation of the DRSi system consists of a wheeled cabinet housing the light source, DAQ, spectrometer and galvo power supply. Carried on top was the laptop computer running the DRSi program and the imager itself.

2.2. Image processing

Image processing in this DRSi system consists of background subtraction followed by spatial and spectral normalization. The image background consists of back reflections from optics in the system and any constant stray light that travels into the collection arm. The background was acquired as an image of a highly absorbing, non-scattering material in contact with the curvature matching window and was subtracted from all subsequent images. Light delivery and signal collection efficiency in DRSi is a function of the imaging lens' numerical aperture (NA) and, to a lesser degree, of the scan mirror size and position. The scan mirror size affects the NA as it dictates the diameter of the collection f-stop. Spatial intensity heterogeneities due to scan angle effects are accounted for by imaging a homogeneous sample used to normalize these effects. For this purpose, a PDMS sample infused with titanium dioxide (TiO_2) for scattering (1mg/mL) was used as a reflectance standard to spatially and spectrally normalize subsequent tissue images. Equation (1) describes the culmination of these normalization operations that result in reflectance images.

$$R(x,y,\lambda) = \frac{\left(I_{Tissue}(x,y,\lambda) - I_{Bkg}(x,y,\lambda)\right)}{\left(I_{\text{Standard}}(x,y,\lambda) - I_{Bkg}(x,y,\lambda)\right)} \tag{1}$$

The spectral reflectance of TiO_2 is largely invariant with wavelength for the concentration and spectral range (450-700nm) used in DRSi images. This point was confirmed by comparing the reflectance of a NIST traceable spectrtalon to that of the TiO2-PDMS standard using a DRS point probe (in contact with the TiO2-PDMS surface). The PDMS standard provides a reference that accounts for any spatial and spectral heterogeneities across the field of view (FOV). The TiO_2 reflectance value was calculated in Eq. (2).

$$R_{TiO2} = \frac{\left(I_{TiO_2} - I_{Bkg}\right)}{\left(I_{\text{Spectralon}} - I_{Bkg}\right)} \tag{2}$$

#199437 - $15.00 USD Received 14 Oct 2013; revised 6 Dec 2013; accepted 9 Jan 2014; published 24 Jan 2014

2.3. Image fitting

There are multiple ways to glean optical and physiological properties from a diffuse reflectance spectrum. We employed the look-up table (LUT) method [19]. The LUT is essentially a database of reflectance spectra for all physiologically relevant absorption (μ_a) and scattering (μ'_s) coefficients; the LUT was numerically fitted to measured reflectance spectra from skin in order to extract μ_a and μ_s'. We have previously applied the LUT method for a variety of applications [7, 19]. We used the LUT method to obtain optical property maps of reduced scattering (μ_s' at 630nm), blood volume fraction and melanin content.

At the image fitting stage, the LUT was numerically fit to the diffuse reflectance spectrum of each pixel, yielding optical property values for that particular pixel. The fitting was performed using custom algorithms written in MATLAB that employ non-linear fitting techniques to minimize the error between the LUT and the measured data. With the data combined from all the pixels, a two-dimensional map was obtained for each optical property. The fitting step was performed offline, as reflectance spectra typically takes about one second per spectra to fit; although several methods exist to speed this process up several orders of magnitude [20].

2.4 System validation

DRSi requires a consistent sampling geometry across the full field in order to accurately capture optical properties across the field of view. This had to be verified in order to be assured that skin image contrast was due only to scattering and absorption heterogeneities. This verification was simply made by measuring the size and center to center separation between the source and collection apertures. To accomplish this, the on-board camera was used to snap images of the sampling geometry at nine points across the field of view. The images were analyzed to see if the size and distance metrics of SDs remained constant or not.

To test for accurate optical property estimation, we imaged a set of phantoms representing a range of reduced scattering and absorption and used them to build an LUT of reflectance. For this set of phantoms, polystyrene beads (Polysciences) and red food dye (McCormick) were used to provide scattering and absorption, respectively. The average spectra of all pixels within each phantom image were averaged, and the resulting spectra were used to build the LUT. After building the LUT model, optical property estimation performance was evaluated after measuring a validation set of phantoms spanning biologically relevant ranges of μ_a and μ_s', where hemoglobin was used as the chromophore. Using the average reflectance spectrum of each phantom image, we fit the LUT to each resulting spectra of known optical properties in order to validate our system.

Lastly, spatial resolution was empirically measured by imaging a turbid material containing fine, well defined contrasting features. Using the edge of the contrasting features as a spatial step function, the step response to that feature edge was analyzed to calculate the line spread function.

2.5 Clinical data collection

The DRSi probe has been used to image the optical property characteristics of skin cancer along lesion margins *in vivo* at the University Medical Center Brackenridge (Seton Hospital). For each lesion, a camera image was taken for co-registration purposes prior to scanning. Each hyperspectral DRSi image was post processed to attain optical property maps of scattering, hemoglobin, and melanin concentration. The institutional review board at the University of Texas at Austin approved the study protocol, and informed consent was received from all patients that participated.

#199437 - $15.00 USD Received 14 Oct 2013; revised 6 Dec 2013; accepted 9 Jan 2014; published 24 Jan 2014

3. Results

3.1. Source-collection geometry

For images of homogeneous phantoms, each reflectance image pixel should ideally be the same in order for optical property maps to be accurate. If this criteria was met (within the statistical variation of the signal due only to shot and dark current noise), then any contrast within the image was attributable only to variations within the tissue. However, in any beam scanning system, there will be artifacts and aberrations; in the case of DRSi, the main artifact was field curvature. To mitigate field curvature effects, existing solutions include f-theta scan lenses that effectively reduce the effect of field curvature through a series of meniscus lenses. A cost effective solution used in DRSi was to match the field curvature to the surface of the skin to be imaged. This was achieved through using a field curvature matching window (plano-convex lens), which was in contact with the tissue. The convex shape of the matching window provides additional functional versatility; concave skin topography (neck, back) can be imaged. This was visually illustrated in Fig. 4, where the results for TracePro simulations for planar and plano-convex matching windows are shown. In this simulation, the difference between the two types of windows was quite pronounced – for the planar case, the beam profiles are very different and highly dependent upon spot location; however, for the plano-convex lens, the beam profile was quite invariant with spot location. Therefore, the plano-convex lens was a very useful, cost-effective solution for imaging skin lesions, which are distributed all over the body.

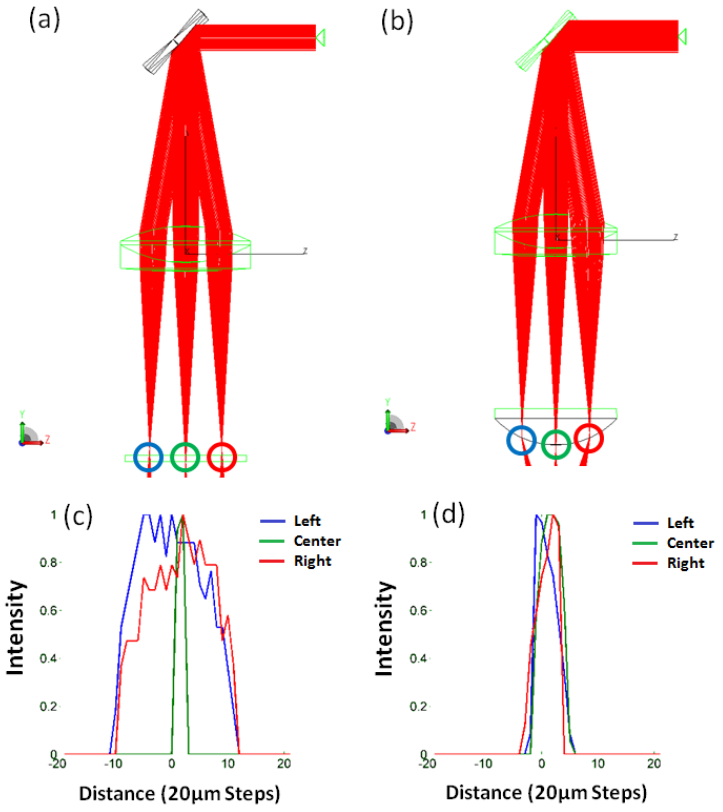

Fig. 4. Focal Plane Matching Ability – Convex vs. Planar Windows. (a) and (b) Raytrace of optical paths containing the planar window (a), and a convex curvature matching window (b). Simulated rays are colored red. (c) and (d) show intensity profiles of spot locations marked by blue, green and red circles for the planar (c) and convex (d) windows.

#199437 - $15.00 USD Received 14 Oct 2013; revised 6 Dec 2013; accepted 9 Jan 2014; published 24 Jan 2014

To empirically validate the curvature compensation shown in the optical simulation, visual inspection of the sampling geometry at various points of scan was performed. By covering the curvature matching window with light adhesive putty, the embedded camera of the DRSi system was used to snap pictures of the source and collection apertures. Light was then sent in through the source and collection fiber ports with the shutter open so that the apertures were visible. Using nine different scan positions, the images of the apertures were used to measure the projection of intensity in the vertical and horizontal directions. After normalization of the projection profiles, it was clear that the size and location of the source and collector apertures are virtually unaffected by scan position, Fig. 5.

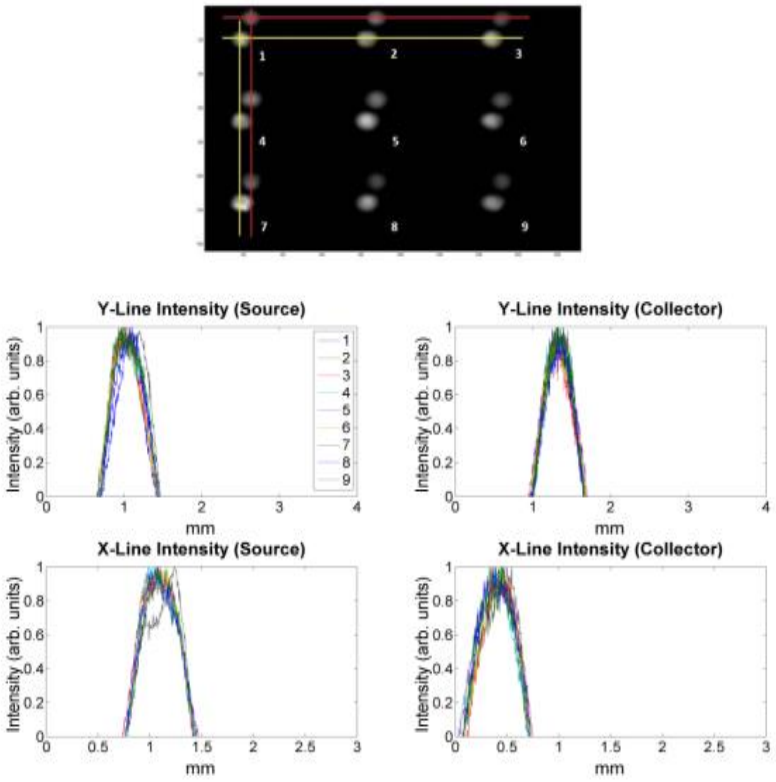

Fig. 5. Source and Collector aperture size and location measurement

The results of these experiments show that the field curvature matching window reduces the effect of field curvature by enabling the sample to be located along a curved surface that closely matches that of the focal plane. The mean diameter spot size was 0.44mm and 0.39mm for the source and detector, respectively. Mean SD separation was 0.74mm with a standard deviation of 0.05mm. Without a curvature matching window, or a planar window, the sampling geometry would not be the same across the image and there would be noticeable and radially symmetric field inhomogeneity.

3.2. Validation

A validation set of liquid phantoms was created comprising biologically relevant ranges of scattering and hemoglobin concentration. The phantoms contained polystyrene beads and human lyophilyzed powder to simulate biological scattering and absorption respectfully. The validation phantoms were imaged, processed and fit for reduced scattering (μ_s' – mm^{-1}) and hemoglobin concentration ([Hb] – mg/mL). The results of the validation are shown in Fig. 6

#199437 - $15.00 USD Received 14 Oct 2013; revised 6 Dec 2013; accepted 9 Jan 2014; published 24 Jan 2014

with the blue line representing perfect performance. The data shows that as an average of all nine validation phantoms, the DRSi system was able to capture scattering and hemoglobin concentration properties to within 5.14% and 8.13% error, respectively.

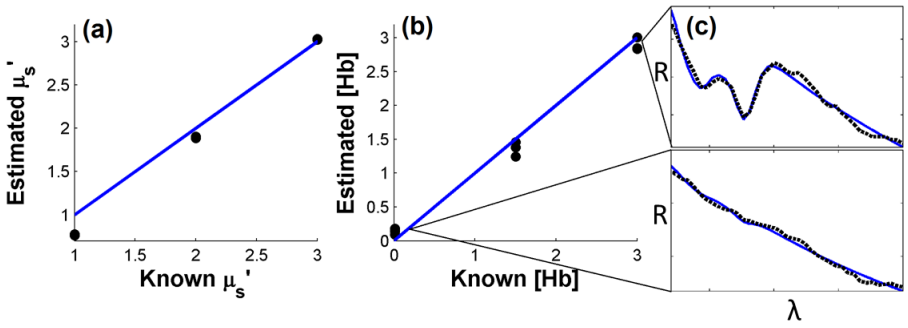

Fig. 6. Optical and physiological property validation for the DRSi system. (a) μ_s' fitting performance. (b) [Hb] fitting performance. (c) Representative raw spectra (black broken lines) with model fits (solid blue lines).

The range of μ_s' and [Hb] used for validation were chosen based on a previous clinical study pertaining to the diffuse reflectance of skin [21]. In that study, skin was found to have μ_s' in the range of 1.91 +/– 0.28 mm^{-1} and blood volume fraction 1.74 +/– 1.42% (corresponding to 2.61 +/– 2.13 mg/ml); concentrations well represented in the this range were used here.

3.3 Spatial resolution

Spatial resolution is typically measured with a United States Air Force (USAF) target of small lines and squares of various sizes. However, due to the nature of the DRSi system and its curvature matching window, imaging a USAF target was difficult to perform accurately unless a properly curved target could be found. Instead we imaged a single square of electrical tape on curvature-matched PDMS so that the edge profile in the horizontal and vertical directions could be measured and the line spread function (LSF) calculated. The LSF was a parameter used to describe image sharpness or resolution in systems where it was less convenient to create a sample containing a point source from which to calculate the point spread function (PSF). In order to calculate the LSF, the edge response, or step profile of a sharp edge in the image needed to be measured. Then once the step response was acquired, its derivative was calculated, giving the LSF (Fig. 7). As with the PSF, the LSF was characterized by the full width half maximum (FWHM) of its pseudo-Gaussian shape, revealing the minimum distance that two features can be separated by and still be distinguished as separate features. As a consequence of this resolution measurement, from the Nyquist theorem, the minimum image size (that will retain maximum resolution) was determined as half of this value.

#199437 - $15.00 USD Received 14 Oct 2013; revised 6 Dec 2013; accepted 9 Jan 2014; published 24 Jan 2014

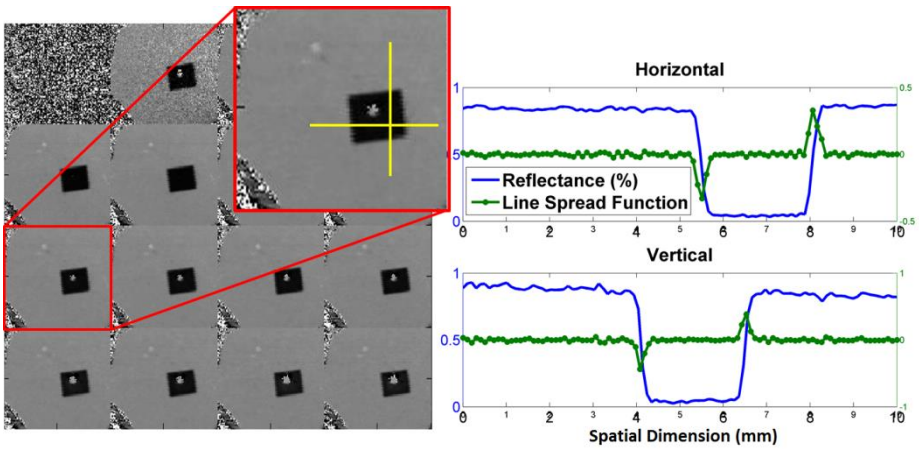

Fig. 7. Reflectance image of a USAF dark square target (left) and the corresponding measured line square functions (right) in the horizontal and vertical directions

The image size used for these measurements was 100x100 pixels, which corresponds to a field of view of 10x10mm. Therefore, the pixel to pixel distance was approximately 100µm. From the LSF measurement, the FWHM of the system resolution was calculated to be approximately 2 pixels or 200µm in both the vertical and horizontal directions. In order to ensure adequate spatial sampling of images with this resolution, the nyquist condition of Eq. (3) must be satisfied,

$$\frac{1}{f_s} = \frac{1}{2 f_c} \tag{3}$$

Where $1/f_s$ was the sampling period and $1/f_c$ was the minimum feature size, or best resolution contained in the image. Therefore, for the DRSi system as configured, the nyquist condition was met if the sampling period was at least 100µm, or half the full width half maximum.

3.4 Skin lesion images

Skin imaging in the clinic was performed in a similar fashion as demonstrated above for the benchtop testing; however, we found it beneficial to apply an index matching gel to the skin surface to avoid some specular reflections prior to acquisition. As stated previously, acquisition time was approximately 50s for the 50x50 pixel image size used, offering a good balance between imaging resolution and acquisition time. Figure 8 shows an example image of an ulcerated basal cell carcinoma (BCC) with the FOV delineated by a white box. Each pixel of the image was fit for concentrations of main chromophores: hemoglobin and melanin where the concentrations are in mg/ml.

#199437 - $15.00 USD Received 14 Oct 2013; revised 6 Dec 2013; accepted 9 Jan 2014; published 24 Jan 2014

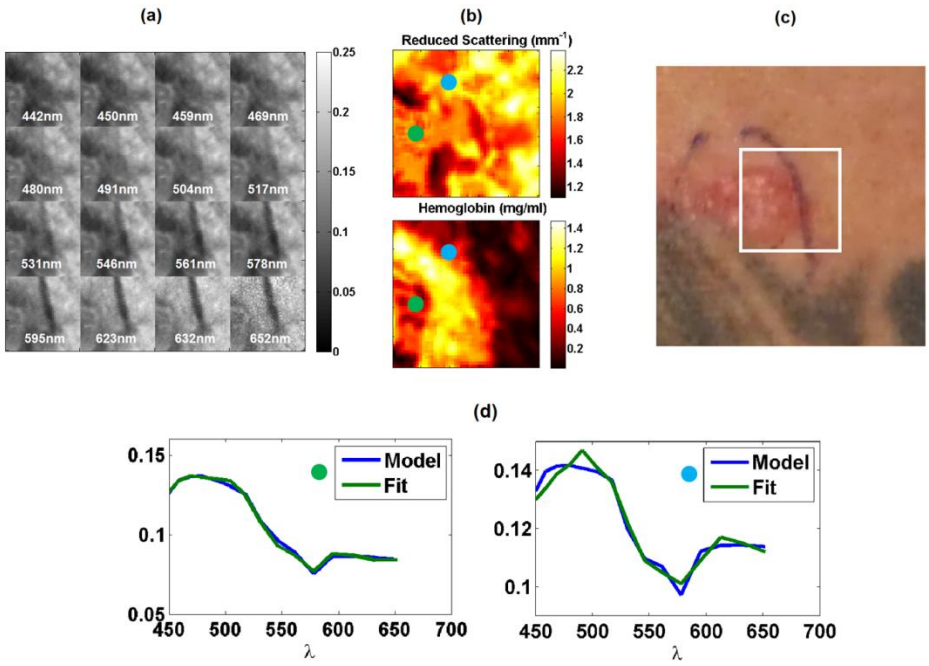

Fig. 8. (a) Hyperspectral diffuse reflectance BCC lesion image and its corresponding reduced scattering (b), reduced scattering and hemoglobin concentration maps. The white square in the camera image (c) denotes the field of view during the image acquisition process. (d) Selected pixel spectra with model fits.

These optical property maps reveal known details about the biochemical nature of skin cancers, but until now have not been revealed through diffuse reflectance modalities. Among these details are the reduction in μ_s' and the increase of hemoglobin concentration, particularly along the lesion margin, which is not always easy for a surgeon to locate. The blue lines surrounding the lesion are pen outlines for demarcation purposes. This pen ink absorption was accounted for in the spectral fit in order to minimize its intrusion into the μ_s' and hemoglobin images. Previous to DRSi, details like these were only discoverable through intricate, invasive histology procedures such as Mohs surgery.

4. Discussion

The DRSi system operation is similar to that of a confocal microscope with a few exceptions. Firstly, the pinhole used in confocal imaging (for removing out-of-focus light) is replaced by the tip of a collection fiber. However instead of collecting single-scattered light from the focal volume, DSRI collects diffusely reflected light offset by a distance 'ρ', from the focal point. This is because while confocal imaging is optimized for spatial confinement of collected photon signal from contrast agents, DRSi is optimized for SNR, and collection of diffuse reflectance. Secondly, the light source used in confocal imaging is a laser (typically UV for fluorescence requiring a long pass filter), which is powerful enough to provide enough single scattering (or fluorophore absorption) events in the focal volume for the required SNR. In contrast, for DRSi, a xenon arc lamp coupled into an optical fiber was used to deliver enough photon flux to the skin to overcome the $1/\rho^2$ attenuation in diffusely reflected light. Broadband optical irradiation and detection in this manner allows for the quantification and decoupling of absorption and scattering based on Photon Transport or Diffusion Theory. Lastly, DSRI is relatively inexpensive compared to Confocal Microscopy (CM); CM requires

#199437 - $15.00 USD Received 14 Oct 2013; revised 6 Dec 2013; accepted 9 Jan 2014; published 24 Jan 2014

higher magnifications and more precise optics, which increases the cost of the imaging system.

Previous clinical studies with point-probe DRS have shown skin cancer lesions to have reduced hemoglobin content and increased scattering compared to normal tissue [2, 18]. As evidenced by the BCC DRSi images of Fig. 8, the result of the imaging approach is consistent with that of single point-sampling. By being able to visualize lesion margins, DRSi could be a powerful tool for image guided skin cancer treatment/removal with minimal involvement with surrounding normal skin.

The DRSi system as described in this paper was optimized for acquisition time and SNR. Increasing the source-collector separation will increase the mean penetration depth of sampled photons; however, the trade-off is reduced sampling efficiency as the diffuse reflectance signal is inversely proportional to the square of the source-collector distance. To compromise, the source-collector separation could be brought down to zero (overlapping), with specular and single scattered light rejected by using cross-polarization methods. Since overlapping sampling geometry retains the optical confinement of sampled photons, optical property derivation is still possible with this configuration. Another benefit of using overlapping source-collector apertures is that shadow artifacts (derived from the SD apertues scanning across a sharp feature) can be avoided [22]. What makes DRSi a unique optical imaging system is that the contrast of each optical property image pixel is dependent on the spectral features derived from the volume it represents. To fit an LUT model to each spectra of the image for light transport in turbid media, the Levenberg Marquardt method of error optimization was used and has been shown to be highly reliable. The SNR also affects the quality of property maps and is a function of detector sensitivity, optical efficiency, light source intensity, and the optical properties of the skin under investigation.

For clinical application, a major limiting factor for performance was the acquisition rate. Increases in image resolution come at the cost of acquisition time. For that reason, a resolution of 50x50 pixels was used for an acquisition time of approximately 50 seconds. Despite the spatial under sampling, the practical usefulness of DRSi images was unaffected as the smallest features that need to be resolved are that of the lesion margins which can vary widely with dimensions of <0.5mm to >10mm: an order of magnitude larger than the resolution of the system. Acquisition times of beyond 60s may result in patient discomfort, motion artifact, and probe pressure effects. Acquisition rates can be improved through more sensitive CCD spectrometers and higher intensity light sources such as supercontinuum lasers; however, this comes with added cost, size and weight. The current hardware provides 50x50 pixel hyperspectral images at 50 seconds per image with 25ms integration times and no averaging. When optimized for speed (integration time = 1ms), this rate drops to 12 seconds with the bulk of time spent on digital to analog (D-A) conversion of the scan signal. Even the D-A conversion time can be reduced through more expensive DAQ hardware (NI PXIe-6356) which we have used to scan 100x100 fields at rates of up to 5 frames per second. To improve the spectral fitting rate, real-time fitting of hyperspectral data sets have been demonstrated with graphical processing unit (GPU) processing, offering speed-ups of over three orders of magnitude [23]. GPU processing is beneficial for hyperspectral data cube fitting due to the highly parallel nature of the GPU, with some units having hundreds of cores.

5. Conclusions

Here we have presented a spatially resolved diffuse reflectance spectroscopy instrument towards the detection of skin cancers *in vivo*. With this instrument, hyperspectral images of turbid media are acquired and the spectra of each pixel was fit for optical and physiological properties. Validation of this system for the fitting of optical properties was accomplished through the use of liquid phantoms that span a range of biologically relevant optical and physiological properties. Image quality was achieved through background subtraction, spatial and spectral normalization and cross polarization.

#199437 - $15.00 USD Received 14 Oct 2013; revised 6 Dec 2013; accepted 9 Jan 2014; published 24 Jan 2014

Advancements in acquisition hardware has reduced the size and cost restraints on this system, making it more readily adaptable to clinical settings and low resource facilities. As digital hardware solutions progress, the tradeoffs in performance that had to be sacrificed can be slowly regained and optical biopsy solutions such as DRSi can be further miniaturized.

By expanding the nature of DRS from a point probing tool to an imaging platform, the potential of this instrument as a viable skin cancer diagnostic tool is enhanced.

Acknowledgments

This research was supported by the National Institutes of Health (R01CA132032-02W1 and R21 EB015892) and the Texas Higher Education Coordinating Board.

#199437 - $15.00 USD Received 14 Oct 2013; revised 6 Dec 2013; accepted 9 Jan 2014; published 24 Jan 2014